J Mater Sci (2008) 43:2990–3000
DOI 10.1007/s10853-007-2164-y

INTERFACE SCIENCE

Effect of single-step strain and annealing on grain boundary character distribution and intergranular corrosion in Alloy 690

Shuang Xia · Bangxin Zhou · Wenjue Chen

Received: 14 June 2007 / Accepted: 13 September 2007 / Published online: 9 October 2007

Abstract The effects of single-step thermomechanical treatments on the grain boundary character distribution (GBCD) and intergranular corrosion of Alloy 690 (Ni–30Cr–10Fe, wt.%) are investigated. High proportion of low ΣCSL grain boundaries (more than 70% according to Palumbo–Aust criterion) associating with large size grains-cluster microstructure is obtained through one-step thermomechanical treatment of 5% cold rolling followed by annealing at 1,100 °C for 5 min. Nucleation density of recrystallization and multiple twinning are the key factors affecting the GBCD. The grains-cluster is produced by multiple twinning starting from a single recrystallization nucleus. That the mean size of the grains-clusters and proportion of low ΣCSL boundaries decrease with the increasing strain, is caused by the increasing nucleation density of recrystallization with the increase of strain. The specimen with large size grains-cluster microstructure and high proportion of low ΣCSL boundaries exhibits much better resistance to mass loss during intergranular corrosion testing than that with small size grains-cluster microstructure and relatively low proportion of low ΣCSL boundaries.

Introduction

Due to its excellent corrosion resistance, nickel based Alloy 690 (Ni–30Cr–10Fe, mass %) is used in corrosive and high temperature applications, such as in the petrochemical and the nuclear industries [1, 2]. But with the prolonged service life and improved performance being demanded by industries, the improvement of the resistance to intergranular attack in Alloy 690 should be considered.

Grain boundary structure has long been known to play a critical role in many material properties, such as precipitation [3, 4], corrosion [5, 6], and cracking [7]. Grain boundary engineering (GBE), which was under the light of "grain boundaries design and control" proposed by Watanabe [8], developed a lot, and was fruitful during the last two decades. The grain boundaries related properties of materials can be enhanced by exercising control over the population of low ΣCSL (Σ≤29) grain boundaries, as defined by the coincident site lattice (CSL) model [9]. A large body of works proved that the grain boundary character distribution (GBCD) can be altered via proper thermomechanical treatments. Some face-centered cubic (fcc) metal materials with low to medium stacking fault energy, such as Pb-base alloy [6, 10], Ni-base alloy [11], OFE copper [12], and austenitic stainless steel [13, 14], were successfully applied this concept to promote $\Sigma 3^n$ (n = 1,2,3…) boundaries formation, and their properties were greatly enhanced. This may be an approach to further improve the resistance to intergranular corrosion of Alloy 690, which is also an fcc material with low stacking fault energy.

Thermomechanical treatments that can increase the proportion of low ΣCSL grain boundaries in this class of materials can be categorized as iterative and single-step thermomechanical treatments [15, 16]. The iterative thermomechanical treatments involve several cycles of strain (mostly less than 30%)/high temperature short anneals [11, 17, 18]. The complexity of this kind of processing makes it difficult to fully understand the mechanism of the GBCD manipulation, and unfavorable for industrial applications.

S. Xia (✉) · B. Zhou · W. Chen
Institute of Materials, Shanghai University, Shanghai 200072, P.R. China
e-mail: xiashuang14@sohu.com

Whether each processing cycle has the same mechanism or different mechanisms in contributing to the GBCD is unclear. And how many cycles of the processing are most favorable is also still not agreed upon by different investigations. So it is very difficult to control this kind of processing. The much simpler single-step processing, which involves relatively small strain, less than 10%, followed by low temperature and long time annealing [13, 14], or high temperature and short time annealing [19–21], is also effective for increasing the proportion of low ΣCSL grain boundaries and enhancing the properties. The processing of single-step strain and high temperature short time annealing will be preferable for industrial applications, since it is much simpler than the iterative processing and does not need long time annealing. However, the mechanism of GBCD alteration by single-step processing is unclear, and how the resulting microstructures affect the material property is also ambiguous.

In this article, the effect of single-step strain followed by high temperature short time annealing on the GBCD and the coexistent microstructure of Alloy 690 were reported. The partial annealed state was observed to interpret the relationship between thermomechanical treatments and resulting GBCD. Finally, the intergranular corrosion testing was carried out on the specimens with different GBCD to reveal how this kind of single-step thermomechanical treatment influences material property.

Experimental procedures

The composition of Alloy 690 used in this study is listed in Table 1. Strip specimens with 10 mm in width, cut from 2 mm thickness plate were vacuum sealed under 5×10^{-3} Pa in quartz capsules and annealed at 1,100 °C for 15 min, then quenched into water and broken quartz capsules (WQ) simultaneously, for the starting material (solution annealed). The GBCD of the starting material is given in Table 2. There are no textures in the starting material, as shown in Fig. 1. Thermomechanical treatments were performed by cold-rolling with the reduction ratio in thickness varying from 5% to 50%, and subsequently annealed at 1,100 °C for 5 min in vacuum sealed quartz capsules, then quenched into water as described above.

Prior to the examination of these specimens, electropolishing was carried out in a solution of 20%$HClO_4$ + 80%CH_3COOH with 30 V direct current. Electron backscatter diffraction (EBSD) was employed for the determination of grain boundary misorientations using the TSL 4.6 laboratories orientation imaging microscopy (OIM) system attached to a Hitachi–S570 scanning electron microscope (SEM) with a tungsten cathode. Operating conditions were: accelerating voltage—20 kV, working distance—25 mm, beam incidence angle—70°. The scans were carried out on a square or rectangular area; with each orientation point being represented as a hexagonal cell, using step sizes about 5–7 μm. According to the differences of grain size in each specimen, the areas analyzed by EBSD had dimensions of approximately $1{,}000 \times 1{,}000$–$1{,}500 \times 1{,}500$ μm^2. Values of the proportion of grain boundaries defined by the CSL model were expressed as a length fraction by dividing the number of hexagonal cells of a particular boundary type with that of the entire grain boundaries. Any adjacent point pair with misorientation exceeding 2° is considered to be a boundary. When analyzing misorientation between crystallites, data points in the middle of grains were used for measurement.

After sensitization treatment at 715 °C for 2 h, the specimens were electropolished to get clear finish surfaces for intergranular corrosion testing. The surface areas of specimens were measured carefully. The specimens were weighed to the nearest 0.01 mg, and then immersed in the solution of 65%HNO_3 + 0.4%HF at room temperature for intergranular corrosion testing. Every 24 h, the specimens were taken out and cleaned by water and ethanol, then dried with warm air. Subsequently the specimens were re-weighed to establish mass loss. The surface morphology of the specimens that undergone intergranular corrosion tests was observed by the same SEM used for EBSD experiment.

Results and discussion

Effect of strain and annealing on GBCD

Table 2 shows the GBCD determined according to Palumbo–Aust criterion [22] of the specimens, which were cold rolled with the reduction of 5–50% and subsequently annealed at 1,100 °C for 5 min and WQ. Alloy 690 is highly propone to twin (Σ3) formation during annealing after strain due to its low stacking fault energy. So Σ3 boundaries made the dominant contribution to the GBCD. When the specimen was annealed at 1,100 °C for 5 min after cold rolled 5%, the proportion of low ΣCSL grain boundaries in Alloy 690 was enhanced to the value in excess of 70%, which comprised about 60% Σ3 boundaries and 9% the summation of Σ9 and Σ27 boundaries. This indicated that small strain and subsequent high temperature

Table 1 Composition of the investigated material (mass %)

Ni	Cr	Fe	C	N	Ti	Al	Si
60.52	28.91	9.45	0.025	0.008	0.4	0.34	0.14

Table 2 Treatment processes and grain boundary character distribution of specimens (Palumbo–Aust criterion)

Specimen number	Cold rolling (%)	Annealing time (min) at 1,100 °C	Σ1(%)	Σ3(%)	Σ9 + Σ27(%)	Other low ΣCSL(%)	Total low ΣCSL ($\Sigma \leq 29$) (%)
Starting material	–	15	3	48.5	2.5	0.5	54.9
A	5	5	1.4	60.1	9.3	0.5	71.3
B	10		2.3	54.2	7.2	0.8	64.5
C	20		2.5	48.8	3.7	0.5	55.5
D	35		4.2	40.3	1.2	1.2	46.9
E	50		4	39.8	1.5	1.4	46.7

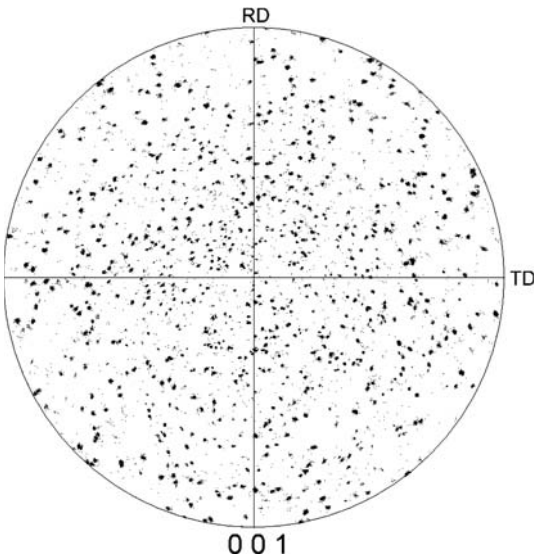

Fig. 1 (001) Pole figure of the starting material (Solution annealed)

annealing will markedly promote annealing twinning and multiple twinning in Alloy 690. When the cold rolling reduction increased from 35 to 50%, the low ΣCSL grain boundary has the lowest occurrence among the investigated specimens. In this case the proportions of Σ3 boundaries are about 40%, and the summation of Σ9 and Σ27 boundaries has very low occurrence, only about one seventh of that of the specimen with the maximum proportion of low ΣCSL grain boundaries. This indicated that multiple twinning events had low probability in the case of large strain. The proportion of $\Sigma 3^n$ boundaries decreased with the increase of cold rolling reduction, which resulted in that the proportion of low ΣCSL boundaries also decrease with the increase of strain. Hence the proportion of low ΣCSL boundaries has a very strong dependence on strain.

The microstructure of the specimens with different GBCD

The OIM map of specimen A, which has the maximum proportion of low ΣCSL grain boundaries is shown in Fig. 2a, and that of specimen C, which has relatively low proportion of low ΣCSL grain boundaries is presented in Fig. 2b. These two OIM maps are given according to Palumbo–Aust criterion. The grains-cluster microstructure is easily identified in Fig. 2a, b. The grains-cluster has the following characteristics: all the boundaries within the cluster can be described by $\Sigma 3^n$ misorientations, whereas the outer boundaries are often crystallographically random with the adjacent grains [23].

For illustrating this kind of microstructure, the misorientations of any two grains within each cluster in Fig. 2a are analyzed. Most of the grain pairs are non-adjacent, and the misorientations of those randomly selected grain pairs are listed in Table 3. It is obvious that the grains within the same cluster have $\Sigma 3^n$ misorientations even when they are at a long distance apart from each other. For example, in Fig. 2a, grains H1 and H2 are in the same cluster H with a size at least of 600 μm, but they also maintain Σ27b misorientation. From grain H1 to grain H2, a line can be drawn only across twin boundaries, thus a long twin chain [24] forms.

The orientation distribution of the grains in the cluster J in Fig. 2a is analyzed in detail, as given in Fig. 3 and Table 4. This cluster contains 29 grains, which are labeled by numbers in Fig. 3a, and their orientations identified on the examination section are shown by color in Fig. 3b. Grains with the same orientation are presented by the same color, as indicated in Fig. 3b, c. There are only 10 different orientations for those 29 grains, i.e., grains 1, 3, 5, 6, 8, 12, and 16 have the same orientation, which is named orientation α; grain 2 has the orientation β; grains 4 and 14 have the same orientation γ; grains 7, 9, 11, 15, 19, and 20 have the same orientation Φ; grains 10 and 21 have the same orientation θ; grains 13, 17, 24, and 26 have the same orientation ε; grains 22, 27, and 29 have the same orientation Ψ; grain 23 has the orientation Ω; grains 18 and 25 have the same orientation δ; grain 28 has the orientation η. The mutual misorientations between these 10 different orientations are shown in Table 4. It is clear that all these orientations have the $\Sigma 3^n$ relationships with each other.

This grains-cluster can be divided into two sub-clusters, which contain grains 1–21 and grains 22–29 respectively.

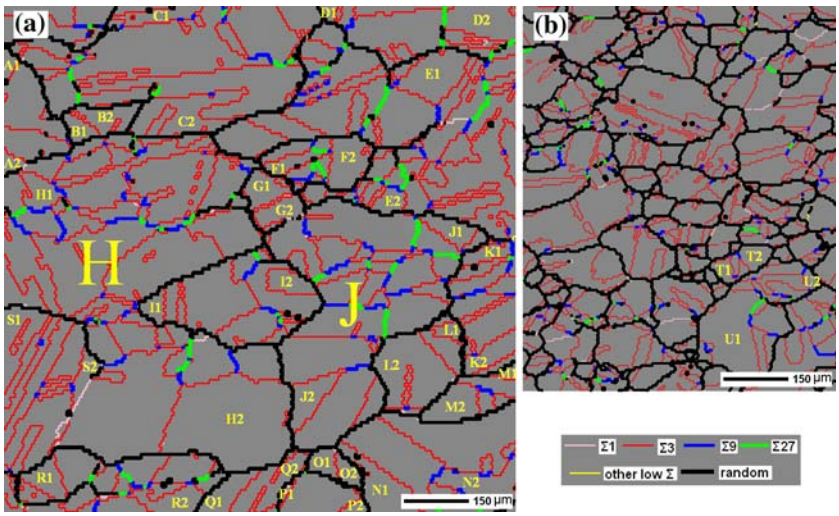

Fig. 2 OIM Maps for specimen A (**a**) and C (**b**). Same letter with different number are in the same grains-cluster

Table 3 Misorientations between grains pairs in same grains-cluster of Fig. 2 and in same twin chain of Fig. 4

Grains pairs	Misorientation	Closest CSL	Deviation ($\Delta\theta$)	$\Delta\theta/\Delta\theta_{max(B)}$	$\Delta\theta/\Delta\theta_{max(P\text{-}A)}$
A1/A2	59.7°[1 1 1]	Σ3	0.4°	0.05	0.07
B1/B2	59.1°[1 1 –1]	Σ3	0.9°	0.10	0.15
C1/C2	59.4°[1 –1 1]	Σ3	0.9°	0.10	0.15
D1/D2	31.0°[0 1 –1]	Σ27a	0.6°	0.21	0.62
E1/E2	31.9°[0 1 1]	Σ27a	0.5°	0.17	0.52
F1/F2	38.1°[1 1 0]	Σ9	1.1°	0.22	0.45
G1/G2	0.5°[–8 7 12]	Same orientation			
H1/H2	35.0°[–1 2 0]	Σ27b	1.0°	0.35	1.03
I1/I2	35.1°[0 1 2]	Σ27b	0.7°	0.24	0.72
J1/J2	38.7°[–1 0 –1]	Σ9	0.4°	0.08	0.17
K1/K2	35.4°[–1 2 0]	Σ27b	0.1°	0.03	0.10
L1/L2	39.6°[0 1 –1]	Σ9	0.8°	0.16	0.33
M1/M2	0.3°[9 24 –10]	Same orientation			
N1/N2	59.6°[1 1 –1]	Σ3	0.6°	0.07	0.1
O1/O2	59.8°[1 –1 1]	Σ3	0.5°	0.06	0.08
P1/P2	39.8°[0 1 1]	Σ9	1.1°	0.22	0.46
Q1/Q2	59.8°[–1 1 1]	Σ3	0.2°	0.02	0.03
R1/R2	35.8°[0 2 –1]	Σ27b	0.7°	0.24	0.72
S1/S2	59.9°[–1 –1 –1]	Σ3	0.7°	0.08	0.12
T1/T2	59.3°[1 1 1]	Σ3	0.7°	0.08	0.12
U1/U2	39.4°[–1 0 1]	Σ9	0.5°	0.1	0.21
V1/V2	35.4°[0 –2 1]	Σ27b	0.2°	0.07	0.21
W1/W2	59.8°[–1 1 1]	Σ3	0.8°	0.09	0.13
X1/X2	59.5°[1 –1 1]	Σ3	0.5°	0.06	0.08
Average value				0.13	0.30

The two sub-clusters are separated by the high order $\Sigma 3^n$ boundaries, i.e., the Σ9 boundaries between grain 15 and grain 22, and between grain 20 and grain 22; the Σ27 boundaries between grain 16 and grain 22, and between grain 21 and grain 22. Among the grains in each sub-cluster, a line can be drawn only cross twin boundaries from any grain to any other grain. Thus the twin-chain can link any two grains in each sub-cluster. But between the grains belonging to different sub-cluster, the twin chain linking between them is interrupted by one high order $\Sigma 3^n$ boundaries. Nevertheless, some grains located in different sub-clusters have the same orientation. For example, grains

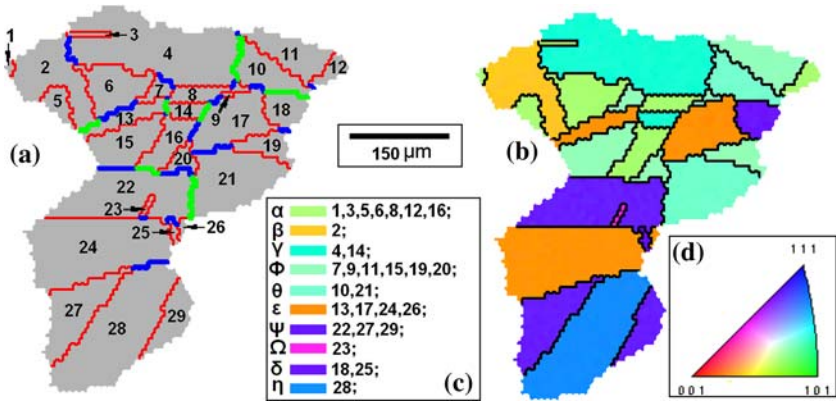

Fig. 3 Orientation distribution of the grains in the cluster J in Fig. 2**a**. (**a**) Grains labeled by number (Boundaries colors are as in Fig. 2), (**b**) Orientation distribution of the grains, (**c**) Color code for the same orientation grains, (**d**) Inverse pole figure for color code

13 and 17 belong to one sub-cluster, and grains 24 and 26 belong to the other one, they also have the same orientation. The OIM map analyzed here represents a two-dimensional section of a three dimensional microstructure, it is highly probable that the twin chain in fact connected below or above the examined surface. Since the higher order $\Sigma 3^n$ boundaries are produced by impingement of twins [24].

In Fig. 2b, which is the OIM map of specimen C, the grains-cluster feature of microstructure is also easily identified. For example, the misorientations of grain pairs T1 and T2, and U1 and U2 were also of $\Sigma 3^n$ type, as listed in Table 3. Comparing Fig. 2a and b, it is easy to see that the mean size of grains-cluster in Fig. 2a is much larger than that of Fig. 2b, although the size of the clusters in Fig. 2a is quite inhomogeneous. To study the dependence of the size of grains-cluster on the treatment process, the mean size of clusters in specimens of Table 2 was evaluated by mean distance between random boundaries intersected by line scan of 3,000 μm for 3 times in different areas by EBSD. The result shown in Fig. 4 is that the mean sizes of the grains-clusters decrease with the increase of the cold rolling reduction. Correspondingly, large grains-cluster microstructure has a high proportion of $\Sigma 3^n$ boundaries, while small grains-cluster microstructure has relatively low proportion of $\Sigma 3^n$ boundaries, as shown in Fig. 4 and Table 2.

The microstructure in the partially recrystallized state

All the investigated specimens annealed at 1,100 °C for 5 min were fully recrystallized. It is conceivable that the microstructure evolution during annealing after strain should be responsible for the variation of the resulting microstructures and GBCD. So the microstructures before full recrystallization are of great interest to be investigated. Specimens annealed at 1,100 °C/3 min (specimen A*) and 1 min (specimen C*) for 5% and 20% cold rolled respectively, were analyzed by EBSD and the point-to-point correlations (misorientations) were obtained. The average misorientation of individual grains were automatically obtained and shown by color in Fig. 5. From the color code, it can be known that the blue area denote smaller average misorientation in grains, which indicates the recrystallized area, and the unrecrystallized area, which has larger average misorientation in grains, is presented by green or even warmer hue. The recrystallized and non-recrystallized regions were separated by random boundaries. There are a lot of $\Sigma 1$ boundaries (misorientation across them in the range of 2°–15°) and $\Sigma 3$ boundaries in unrecrystallized areas, which are predestined to be wiped off by the growth of recrystallization grains. Therefore, it is meaningless to give statistic of the GBCD for the specimens in the partially recrystallized state.

Most of the recrystallized grains are enwrapped by the non-recrystallized regions in specimen A*, as shown in Fig. 5a. It can be seen that some recrystallized areas contain straight-sided $\Sigma 3$ boundaries, which are annealing twins, while the smaller ones do not contain, and the larger ones contain more. This implies that during the growth of the recrystallized grains by consuming the non-recrystallized regions, continuous chain of twin boundaries can be left behind in the wake of the migrating random boundary, which separated the recrystallized and non-recrystallized regions. We do not touch here, the questions of the mechanisms of twin formation [25–28] and why does the twins continuously form to produce twin chain [24, 29]. We just focus on the question: if twinning takes place continuously to form twin chain, how can it explain the relationship between the thermomechanical treatments and the obtained microstructures.

The twin chains can be easily identified in the partially recrystallized microstructure. For example, in Fig. 5a, the twin chain from grain V1 to V2 involves four twin boundaries; similarly, the twin chain from W1 to W2 involves five twin boundaries. The misorientations of those two grain pairs are listed in Table 3. Most of the areas in

Table 4 Mutual misorientations between 10 different orientations in the grains-cluster of Fig. 3

	α	β	γ	Φ	θ	ε	Ψ	Ω	δ
β	59.5°[1 −1 −1]/Σ3/0.8°								
γ	59.6°[1 1 −1]/Σ3/0.6°	38.7°[1 0 1]/Σ9/0.3°							
Φ	59.7°[1 −1 1]/Σ3/0.7°	38.5°[0 −1 −1]/Σ9/0.6°	39.4°[0 1 1]/Σ9/0.5°						
θ	38.6°[0 1 1]/Σ9/0.5°	35.6°[2 1 0]/Σ27b/0.5°	31.1°[0 −1 −1]/Σ27a/0.6°	59.9°[1 1 1]/Σ3/0.4°					
ε	38.4°[0 −1 1]/Σ9/0.9°	35.9°[−2 0 1]/Σ27b/0.5°	34.9°[2 −1 0]/Σ27b/0.6°	59.8°[−1 1 1]/Σ3/0.5°	38.6°[1 0 1]/Σ9/0.5°				
Ψ	35.8°[0 −2 1]/Σ27b/0.5°	54.8°[2 3 2]/Σ81b	38.6°[−1 1 −4]/Σ81a	38.8°[−1 0 1]/Σ9/0.7°	35.1°[0 2 −1]/Σ27b/0.4°	59.6°[−1 1 −1]/Σ3/0.9°			
Ω	39.0°[−4 1 −1]/Σ81a	49.8°[−3 17 −20]/Σ243b	43.0°[−11 20 −11]/Σ243a	36.1°[1 −2 0]/Σ27b/0.7°	55.1°[−3 −2 −2]/Σ81b	38.7°[0 1 1]/Σ9/0.7°	59.8°[1 −1 1]/Σ3/0.4°		
δ	36.2°[−1 2 0]/Σ27b/0.9°	39.4°[6 25 −6]/Σ81a	54.6°[−2 −2 −3]/Σ81b	38.7°[0 −1 1]/Σ9/0.4°	32.6°[−1 0 −1]/Σ27a/1.0°	59.7°[−1 −1 1]/Σ3/0.5°	39.1°[1 1 0]/Σ9/0.6°	31.6°[21 0 22]/Σ27a/0.6°	
η	39.1°[3 1 5]/Σ81c	34.9°[5 −4 −2]/Σ243d	42.8°[−1 14 −4]/Σ243a	31.7°[1 0 1]/Σ27a/0.3°	38.0°[−1 3 −5]/Σ81c	38.3°[−1 −1 0]/Σ9/0.7°	59.9°[−1 1 1]/Σ3/0.7°	39.7°[1 1 0]/Σ9/0.9°	35.0°[0 −1 −2]/Σ27b/0.7°

Note: Orientation relationships are given in the form: Misorientation/Closest CSL/Deviation; the deviations of Σ>27 cannot be accurately measured by the equipment and not given here

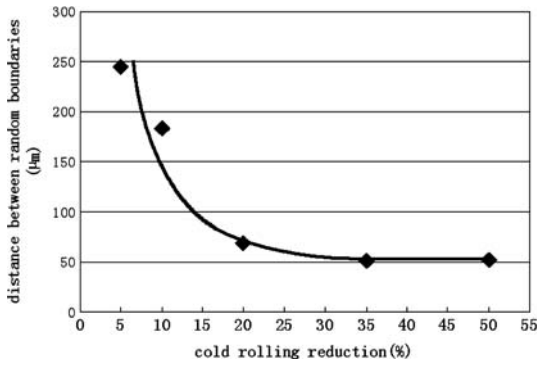

Fig. 4 The relationship between mean dimensions of grains-cluster and the cold rolling reduction

specimen C*, as shown in Fig. 5b are blue, which indicated recrystallized regions. Most of grains-clusters in these regions have already impinged on each other. The twin chains can also be easily identified in the recrystallized regions. For example, the twin chain from grain X1 to X2 involves three twin boundaries, and the misorientations of these two grains are also listed in Table 3. The misorientations of those grain pairs (V1/V2, W1/W2, and X1/X2) are of $\Sigma 3^n$ type, as shown in Table 3. The twin chains in other recrystallized areas of Fig. 5a and b have the similar situation.

Twin chains formed during recrystallization had been studied a lot, and the results were summarized by Berger [29]. Under the light of this knowledge, it is easy to know that each twin chain started from each single orientation, i.e., single recrystallization nucleus. Concurrently, with the formation the twin chain, $\Sigma 3^n$ boundaries were produced by multiple twinning. To clarify the multiple twinning processes, possible formation processes of two recrystallized areas outlined by black framework in Fig. 5a and b are schematically illustrated in Fig. 5c and d respectively. It is only shown that multiple twinning occurs in two dimensions, and it is conceivable that multiple twinning in three dimensions underwent similar process.

The fully recrystallized microstructures of specimen A and C, as shown in Fig. 2a and b, are developed from the partially recrystallized ones, similar to those of specimen A* and C* in Fig 5a and b. Since the starting material is without texture, as shown in Fig. 1, the grains-cluster is extremely unlikely formed by joining two or more twin chains during recrystallization. Rather, the grains-cluster should be developed from a single twin-chain of recrystallization. As analyzed above, the twin-chain is developed from a single recrystallization nucleus. Consequently, the grains-cluster is formed by continuous twinning events starting from a single nucleus of recrystallization, with the associated presence of multiple $\Sigma 3^n$ boundaries. This can explain why the grains in same cluster maintain very close $\Sigma 3^n$ misorentation even at a long distance in Fig. 2.

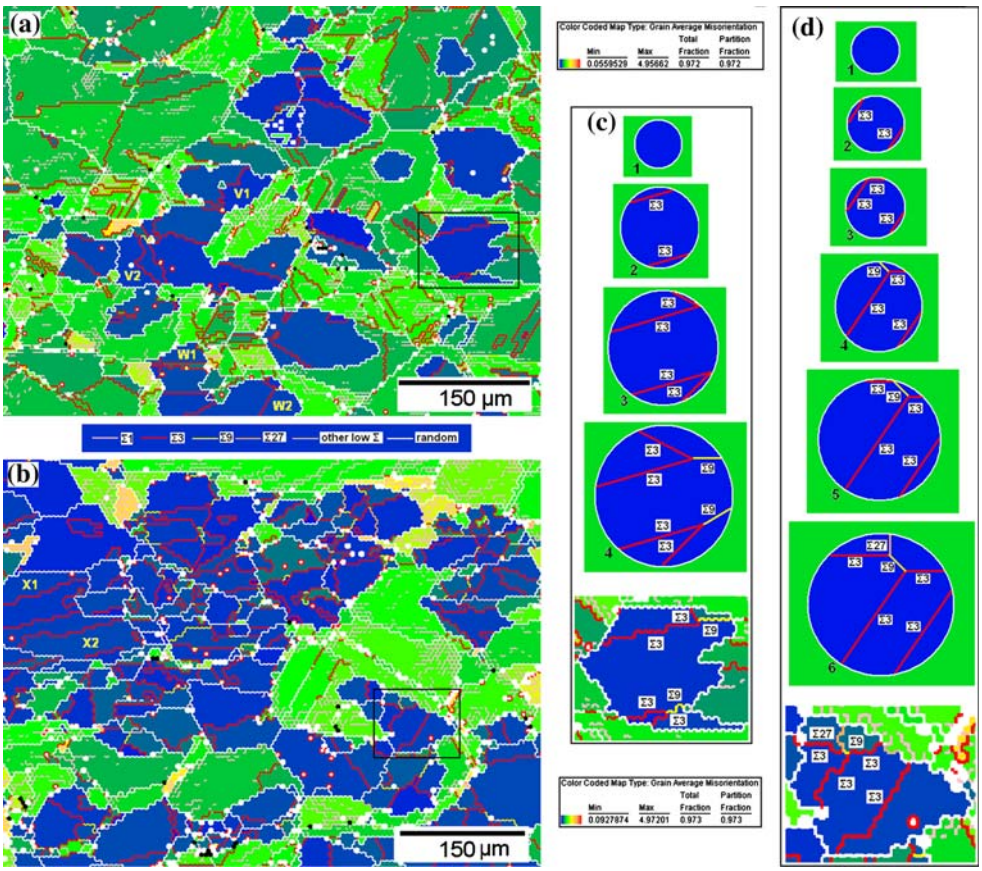

Fig. 5 The OIM maps of partially recrystallized specimens A* (5% cold rolled + 1,100 °C/3 min) and C* (20% cold rolled + 1,100 °C/1 min), (**a**) and (**b**) are the grain average misorientation maps of specimens A* and C*, (**c**) and (**d**) are the schematic illustration of the possible multiple twinning process of the two recrystallized regions outlined by black framework in (**a**) and (**b**) respectively

It is hard to say which grain is the starting nucleus in each twin chains in Fig. 5a and b, but it can be deduced that nucleation density (i.e. the number of nuclei in unit area) of the specimen with 5% strain is much lower than that with 20% strain during annealing. This is according to the common knowledge that smaller strain will result in lower nucleation density during recrystallization [30]. As a consequence, the recrystallization nuclei in the specimen with small strain have much larger area available for growing than those in the specimen with large strain. During growth in larger area, twinning and multiple twinning events have more opportunity to occur, so the size of the grains-cluster and the proportion of $\Sigma 3^n$ boundaries in Fig. 2a are much larger than those in Fig. 2b. Therefore, the proportion of low ΣCSL grain boundaries is high for the specimen with low strain, as shown in Table 2.

In Fig. 2a the size of grains-cluster is quite inhomogeneous. This is caused by that some of these recrystallization nuclei extensively grow to form very large clusters, and others grow to relatively small sizes. In the specimen with small strain, the local orientation will be different with respect to the deformation direction, so stored energy will be inhomogeneous from area to area. As a consequence, nucleation density is inhomogeneous in different areas. Therefore, in Fig. 2a, the size of grains-clusters which developed from each single nucleus is quite inhomogeneous. However, the average nucleation density increases with the increase of strain. So, the mean size of the grains-cluster in the final microstructure and corresponding proportion of low ΣCSL grain boundaries decrease with the increase of strain, as shown in Fig. 4 and Table 2.

The connectivity of random grain boundaries in the microstructure with high proportion of low ΣCSL grain boundaries

From above analysis, it can be known that the proportion of low ΣCSL grain boundaries is enhanced by the formation of large size grains-clusters, which are the result of low nucleation density and multiple twinning. The grains-cluster is formed by twinning or multiple twinning starting from a single recrystallization nucleus. So all the twins and its variant $\Sigma 3^n$ boundaries intrinsically locate inside the grains-cluster, rather than appear in the network of random boundaries as segments to break up its connectivity.

Some articles reported that when the proportion of low ΣCSL grain boundaries was enhanced, the random boundaries network would be substantially fragmented

[20, 31–33], which seemed to be different with the current result. However one point should be noted that the GBCD and OIM maps given above are obtained by applying the Palumbo–Aust criterion. There are two popular criterions in defining the CSL boundaries:

Palumbo–Aust criterion [22]: $\Delta\theta_{\max(P\text{-}A)} = 15^\circ\ \Sigma^{-5/6}$
Brandon criterion [34]: $\Delta\theta_{\max(B)} = 15^\circ\ \Sigma^{-1/2}$

The deviation of experimentally measured misorientation from exact CSL misorientation is denoted by $\Delta\theta$. The deviation degree from exact CSL can be described by a relative deviation [35] $\Delta\theta/\Delta\theta_{\max}$, where the $\Delta\theta_{\max}$ is the maximum permissible deviation. For the Brandon criterion and Palumbo–Aust criterion, the relative deviations are expressed as: $\Delta\theta/\Delta\theta_{\max\ (B)}$ and $\Delta\theta/\Delta\theta_{\max(P\text{–}A)}$, respectively. Only if the value of these parameters is smaller than 1, the examined misorientation was regarded as CSL in the regime of that criterion.

The OIM map of specimen A, which is given according to the Palumbo–Aust criterion in Fig. 2a, is given again in Fig. 6 according to the Brandon criterion. Comparing Fig. 2a with Fig. 6, it can be seen that the connectivity of the random boundaries, which lie between the grains-clusters, is obviously broken up by segments of low ΣCSL grain boundaries after applying the Brandon criterion. For example, the random boundaries around the two grains-clusters I and J in Fig. 6, are markedly broken up by some

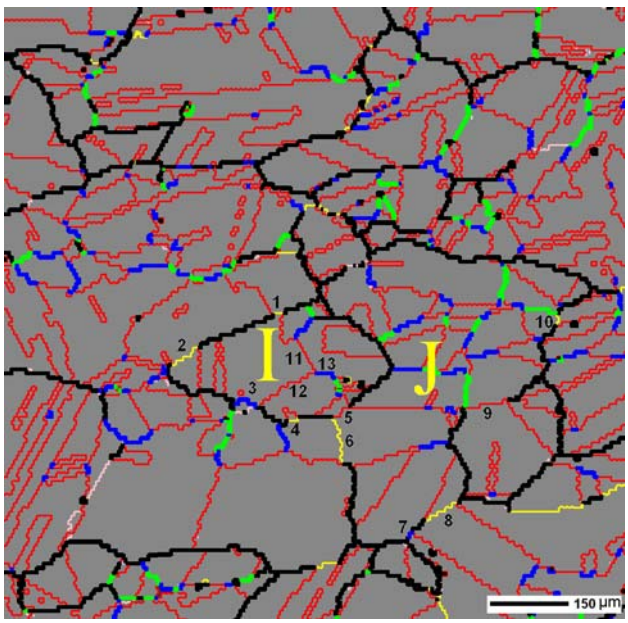

Fig. 6 OIM map for specimen A (Brandon criterion). The connectivity of random boundaries network is substantially interrupted. The interrupter of the random boundaries around two grains-clusters I and J are labeled from 1 to 10. Some boundaries inside the cluster I are also labeled (11, 12, 13). (Boundaries colors are as in Fig. 2)

low ΣCSL grain boundaries numbered 1–10. These 10 boundaries are analyzed in Table 5. For comparing, three boundaries numbered 11–13 inside the cluster I are also analyzed in Table 5. The average values $\Delta\theta/\Delta\theta_{\max(B)}$ and $\Delta\theta/\Delta\theta_{\max(P\text{–}A)}$ of boundaries 1–10 are 0.86 and 1.97 respectively, while these two values of boundaries 11–13 are 0.07 and 0.11, as shown in Table 5. This indicates that the low ΣCSL boundaries that break up the connectivity of the random boundaries have much larger deviation than those located inside the grains-cluster.

To ensure this kind of phenomena, another 60 low ΣCSL boundaries (defined by Brandon criterion) which break up the connectivity of the random boundary network in other area of this OIM map and other OIM maps of specimen A, are also investigated. The results together with the limits of both Brandon and Palumbo–Aust criterion are plotted in Fig. 7. It is obviously that the deviations of most low ΣCSL boundaries interrupt the connectivity of the random boundary network are above the Palumbo–Aust criterion limit. The average values of $\Delta\theta/\Delta\theta_{\max(B)}$ and $\Delta\theta/\Delta\theta_{\max(P\text{–}A)}$ for those boundaries are 0.74 and 1.75 respectively. This indicates that if a boundary segment that breaks up the connectivity of the random boundary is ranked as a low ΣCSL one according to Brandon criterion, it is highly probable that this boundary will be excluded from the low ΣCSL boundary rank according to Palumbo–Aust criterion. For comparison, the average values of $\Delta\theta/\Delta\theta_{\max(B)}$ and $\Delta\theta/\Delta\theta_{\max(P\text{–}A)}$ for the misorientations between grains within each cluster listed in Table 3 are calculated, 0.13 and 0.30 respectively, which are much smaller than those of the boundaries which break up the connectivity of the random boundary network. As analyzed above, the grains-cluster is formed by multiple twinning starting from a single recrystallization nucleus. Since the starting material is without texture, the random boundaries are formed by impingement of unrelated grains-clusters during recrystallization. Therefore, though misorientations of some boundaries between clusters are close to the low ΣCSL (defined by Brandon criterion), they simply happen to be in that situation, and are not geometrically necessary in contrast to the $\Sigma 3^n$ boundaries inside the clusters.

Palumblo, Aust and co-workers [22, 36–38] compared the application of Palumbo–Aust and Brandon criterion in analyzing the experimental results pertaining to interface properties. These results showed that very few boundaries classified as low ΣCSL boundaries according to Palumbo–Aust criterion display attacked, while according to Brandon criterion, more low ΣCSL boundaries display attacked. Therefore, Palumbo–Aust criterion is a better one to define CSL boundaries with special properties. By applying Palumbo–Aust criterion, the connectivity of random boundary network is not substantially broken up in our study as shown in Fig. 2.

Table 5 Misorientations of the boundaries numbered in Fig. 6

Number	Misorientation	Closest CSL	Deviation ($\Delta\theta$)	$\Delta\theta/\Delta\theta_{max(B)}$	$\Delta\theta/\Delta\theta_{max(P\text{-}A)}$
1	46.9°[19 9 21]	Σ29b	2.5°	0.90	2.72
2	46.0°[–6 –7 –13]	Σ21b	2.5°	0.76	2.08
3	41.6°[–19 1 23]	Σ9	4.6°	0.92	1.90
4	47.6°[–20 –21 –1]	Σ11	3.6°	0.80	1.76
5	51.6°[–12 –13 12]	Σ3	8.5°	0.98	1.41
6	47.4°[7 –1 –16]	Σ15	3.6°	0.93	2.28
7	34.8°[–17 –2 –18]	Σ9	4.9°	0.98	2.02
8	38.4°[–1 –1 3]	Σ23	2.1°	0.67	1.89
9	55.1°[8 –9 10]	Σ3	7.1°	0.82	1.18
10	43.9°[0 1 19]	Σ29a	2.3°	0.82	2.50
Average value				0.86	1.97
11	59.8°[1 1 1]	Σ3	0.2°	0.02	0.03
12	59.2°[1 1 1]	Σ3	0.8°	0.09	0.13
13	39.5°[0 1 –1]	Σ9	0.4°	0.08	0.17
Average value				0.07	0.11

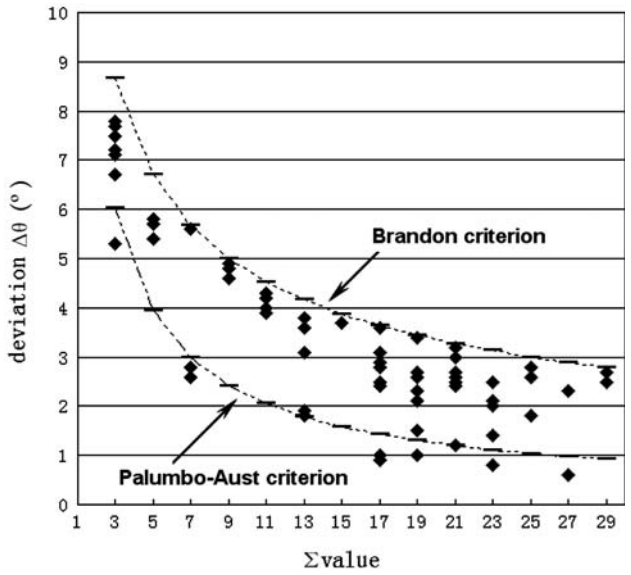

Fig. 7 Deviations of some 60 boundaries (close to low ΣCSL misorientations), which appeared on the random boundaries network in specimen A

The designation of CSL is only based on misorientation. For example Σ3 boundaries are grain boundaries, which have a misorientation within ±8.6° or ±6° of 60°/⟨111⟩ for the Brandon and Palumbo–Aust criterions respectively. The Σ3 family consists of annealing twins (which are symmetrical tilt boundaries characterized by {111} boundary planes), various tilt and twist boundaries (mostly asymmetric tilts or symmetrical) and grain boundaries which happen to have a Σ3 misorientation but generally have irrational or random boundary planes [39]. According to Randle's study [40], for Σ3 boundaries small relative deviation ($\Delta\theta/\Delta\theta_{max}$), mostly associated with {111} boundary plane, which is of coherent twin boundary, while large relative deviation mostly associated with irrational boundary planes. Grain boundaries which happen to have a Σ3 misorientation by impingement of unrelated grains will generally have irrational or random boundary planes. These kinds of boundaries do not exhibit special properties [40–42]. Σ3 boundaries with very large deviations in contrast with those of the twins inside the cluster are also observed in our study, such as boundaries 5 and 9 in Fig. 6. They appear on the network of the random boundaries and break up its connectivity. So this kind of discontinuity of random boundaries is not reliable. Similarly, the deviations of almost all the low ΣCSL boundaries (Brandon criterion) interrupting the random boundary connectivity are comparatively high, as shown in Fig. 7. Hence the marked discontinuity of random boundaries according to Brandon criterion is not reliable.

Intergranular corrosion phenomena in Alloy 690 with different GBCD

It turns out that the connectivity of random boundary network is very sensitive to the criterion of CSL in the present study. The connectivity of random boundaries network is substantially interrupted when the Brandon criterion is applied, whereas not fragmented obviously when the Palumbo–Aust criterion is used. In this instance, whether material property will be enhanced for the specimen with high proportion of low ΣCSL grain boundaries is valuable to be investigated. Specimen A and C were subjected to anneal at 715 °C for 2 h to induce sensitization, which

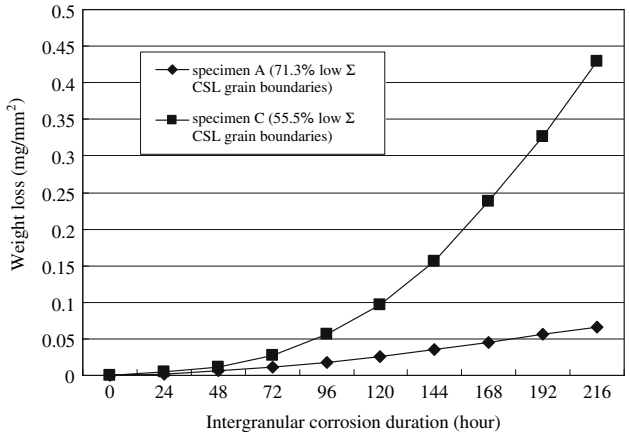

Fig. 8 Weight losses of specimens A and C after sensitization as a function of intergranluar corrosion time

increased the intergranular corrosion susceptibility for intergranular corrosion testing. After sensitization treatment, specimens A and C were applied in intergranular corrosion testing.

Weight losses per area of each specimen as a function of corrosion time are shown in Fig. 8. It is obvious that the weight loss during intergranular corrosion of specimen A is much less than that of specimen C. Surface morphologies of the sensitized specimens A and C undergone 144 h corrosion are shown in Fig. 9a, b and c, d, respectively. In Fig. 9a, which is the surface morphology of specimen A, it is clear that there is a grains-cluster on the point of dropping, and its magnified image is shown in Fig. 9b. In Fig. 9b, the boundaries around the dropping grains-cluster display heavily attacked phenomenon than that of the boundaries inside the cluster. This indicates that the weight loss occurs when individual grains-cluster is removed from the specimen surface, as their surrounding random boundaries are breached by intergranular corrosion. After sensitization treatment, carbide precipitation and associated depletion of Cr are more pronounced in the vicinity of random boundaries than the $\Sigma 3^n$ boundaries inside the cluster. As a consequence, the random boundaries around the grains-cluster are corroded much heavily than the$\Sigma 3^n$ boundaries inside the cluster, as indicated in Fig. 9b.

After 144 h corrosion, most surface area of specimen A is integrated, as shown in Fig. 9a, b, while the surface of specimen C has rather bad integrity, where the dropping phenomena are very serious, as shown in Fig. 9c, d. The differences between specimen A and C are the GBCD and the concurrent size of the grains-cluster, as shown in Table 2, Fig. 2, and Fig. 4. These indicate that large grains-cluster is harder to drop from the specimen surface. Based on these observations, the authors attribute the improvement of resistance to mass loss during intergranular corrosion to the large size of the grains-cluster rather than the unreliable discontinuity of the random boundary network as analyzed in section "The connectivity of random … boundaries".

Firstly, in the large grains-cluster microstructure with high proportion of low ΣCSL grain boundaries, there are less random boundaries available for being heavily attacked in the specimen surface. Secondly, the intergranular corrosion will go a much longer path and take more time to make the large grains-cluster drop than a smaller

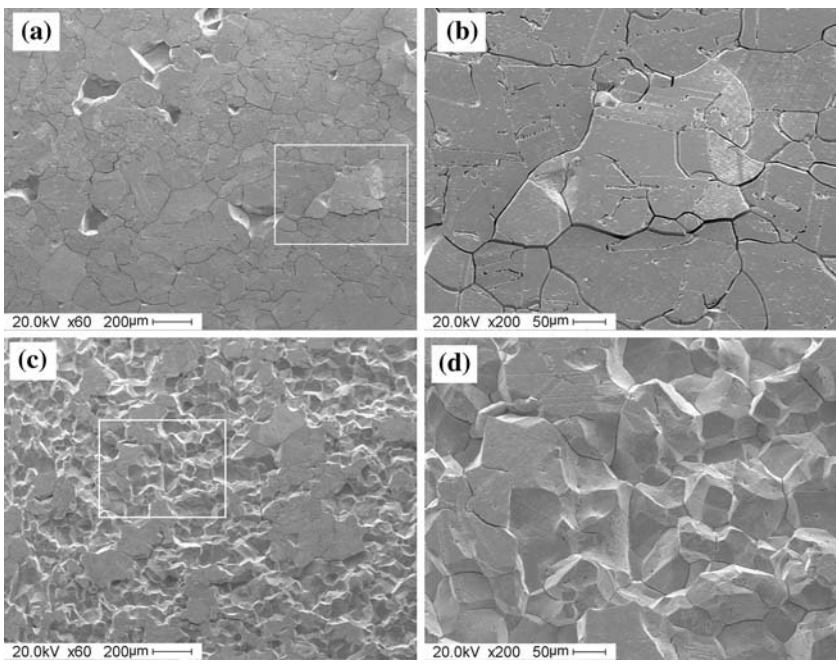

Fig. 9 SEM images of the surfaces of sensitized specimen A (**a**), C (**c**), undergone 144 h intergranular corrosion. (**b**) and (**d**) are the magnified images of the area outlined by white frameworks in (**a**) and (**c**) respectively

one. Thirdly, the large grains-clusters protect the under layer microstructure much better than the smaller ones. Only after the most external clusters drop, the under layer microstructure will suffer as aggressive solution as the external ones do. The small clusters are quicker to drop, and then undersurface clusters are quicker to suffer the corrosive environment. So the weight loss for specimen with small grains-clusters is much severe than that with large ones, as being presented in Fig. 8.

Summary and conclusions

(1) In Alloy 690, small strain (5%) and subsequent high temperature (1,100 °C) annealing for short time (5 min) can produce high proportion of low ΣCSL grain boundaries (more than 70%), which mainly are $\Sigma 3^n$. In this case, the large size twin-induced grains-cluster constitute the microstructure.

(2) Based on the observation of partial and full recrystallization state, it is clear that the nucleation density and multiple twinning are the key factors affecting the GBCD. The grains-cluster is formed by continuous chain of twinning events starting from a single nucleus of recrystallization, and with the associated presence of multiple $\Sigma 3^n$ boundaries. As a consequence, all the grains inside the same cluster have close $\Sigma 3^n$ misorientations even at a long distance. The size of the grains-clusters and the proportion of $\Sigma 3^n$ boundaries decreases with the increase of cold rolling reduction. This is the result of that nucleation density of recrystallization increases with the increase of strain.

(3) In the case of high proportion of low ΣCSL boundaries, connectivity of random boundaries network is very sensitive to the applied criterion of CSL. The connectivity of random boundary network is not fragmented obviously when the Palumbo–Aust criterion is used, whereas substantially interrupted when the Brandon criterion is applied. Almost all those low ΣCSL boundaries (Brandon criterion) appear on the network of the random boundaries have very large deviations. Hence, the high resistance to mass loss during intergranular corrosion testing is attributed to the large size of the grains-cluster accompanied with high proportion of low ΣCSL boundaries, rather than the unreliable discontinuity of the random boundary network.

Acknowledgements This work was supported by Major State Basic Research Development Program of China (2006CB605001) and Shanghai leading academic discipline project (T0101).

References

1. Thuvander M, Stiller K (2000) Mat Sci Eng A 281:96–103
2. Qiu S, Su X, Wen Y (1995) Nuclear Power Engineering 16: 336–340
3. Kurban M, Erb U, Aust KT (2006) Scripta Mater 54:1053–1058
4. Bi HY, Kokawa H, Wang ZJ (2003) Scripta Mater 49:219–223
5. Bennett BW, Pickering HW (1987) Metall Trans A 18A:1117–1124
6. Palumbo G, Erb U (1999) MRS Bull 24:27–32
7. Crawford DC, Was GS (1992) Metall Trans A 23A:1195–1206
8. Watanabe T (1984) Res Mech 11:47–82
9. Kronberg ML, Wilson FH (1949) Trans Am Inst Min Engrs 185:501
10. Lehockey EM, Limoges D, Palumbo G, Sklarchuk J, Tomantschger K, Vincze A (1999) J Power Sources 78:79–83
11. Lin P, Palumbo G, Erb U (1995) Scripta Metall Mater 33:1387–1392
12. King WE, Schwartz AJ (1998) Scripta Mater 38:449–455
13. Shimada M, Kokawa H, Wang ZJ (2002) Acta Mater 50:2331–2341
14. Michiuchi M, Kokawa H, Wang ZJ, Sato YS, Sakai K (2006) Acta Mater 554:5179–5184
15. Randle V (2004) Acta Mater 52:4067–4081
16. Randle V (1999) Acta Mater 47:4187–4196
17. Kumar M, Schwartz AJ, King WE (2002) Acta Mater 50:2599–2612
18. Alexandreanu B, Capell B, Was G (2001) Mat Sci Eng A 300: 94–104
19. Lee S-L, Richards NL (2005) Mat Sci Eng A 390:81–87
20. Guyot BM, Richards NL (2005) Mat Sci Eng A 395:87–97
21. Tan L, Sridharan K, Allen TR (2006) J Nucl Mater 348:263–271
22. Palumbo G, Aust KT (1990) Acta Metall Mater 38:2343–2352
23. Gertsman VY, Henager CH (2003) Interface Sci 11:403–415
24. Gottstein G (1984) Acta Metall 32:1117–1138
25. Fullman RL, Fisher JC (1951) J Appl Phys 22:1350–1355
26. Gleiter H (1969) Acta Metall 17:1421–1428
27. Meyers MA, Murr LE (1978) Acta Metall 26:951–962
28. Mahajan S, Pande CS, Imam MA, Rath BB (1997) Acta Mater 45:2633–2638
29. Berger A, Wilbrandt P-J, Ernst F (1988) Prog Mater Sci 32:1–95
30. Humphreys FJ, Hatherly M (2004) Recrystallization and related annealing phenomena, 2nd ed. Elsevier, Oxford
31. Kumar M, King WE, Schwartz AJ (2000) Acta Mater 48:2081–2091
32. Schuh CA, Kumar M, King WE (2003) Acta Mater 51:678–700
33. Schuh CA, Kumar M, King WE (2003) Z Metallkd 94:323–328
34. Brandon DG (1966) Acta Metall 14:1479–1484
35. Randle V (1996) The role of the coincidence site lattice in grain boundary engineering. Cambridge University, Cambridge, UK
36. Palumbo G, Aust KT, Lehockey EM (1998) Script Mater 38:1685–1690
37. Kim SH, Erb U, Aust KT, Palumbo G (2001) Script Mater 44:835–839
38. Zhou Y, Aust KT, Erb U, Palumbo G (2001) Script Mater 45:49–54
39. Randle V, Davies H (2002) Ultramicroscopy 90:153–162
40. Randle V, Davies P (1999) Interface Sci 7:5–13
41. Gertsman VY, Bruemmer SM (2001) Acta Mater 49:1589–1598
42. Lin H, Pope DP (1993) Acta Metall Mater 41:553–562